An analytical solution for rapidly distorted turbulent shear flow in a rotating frame

E. Akylas,[a] S. C. Kassinos,[b] and C. A. Langer
Department of Mechanical and Manufacturing Engineering, University of Cyprus, 75 Kallipoleos, Nicosia 1678, Cyprus

(Received 15 April 2006; accepted 28 June 2006; published online 17 August 2006)

In this study we apply rapid distortion theory to the case of nonstratified homogeneous turbulence that is sheared in a frame that counter-rotates at a rate that matches in magnitude the rotation associated with the mean shear. In the inviscid case, analytical solutions are worked out for the evolution of the components of the Reynolds stresses and the structure dimensionality tensor, and these are shown to equal each other. The results are compared to direct numerical simulations data with which they proved to be in good agreement, especially in terms of the Reynolds shear stress and of the dimensionless tensor components. Finally, the development of the structure of a passive scalar field with a constant mean gradient is investigated, and remarkable analogies are shown to exist between this case and the case of shear in a fixed frame.
[DOI: 10.1063/1.2265010]

I. INTRODUCTION

The effects of system rotation on turbulent shear flows have received considerable attention during the last decade because of their relevance to important technological and astrophysical problems, such as turbomachinery flows and the accretion of stellar disks. In the nonrotating case, it is well documented that homogeneous mean shear tends to elongate and align the turbulence structures in the direction of the mean flow (Rogers and Moin[1]). In fact, Lee *et al.*[2] used direct numerical simulations (DNS) to study homogeneous shear flow at high shear rates, and observed streaky turbulent structures that were reminiscent of the structures found in turbulent boundary layers. Early numerical studies, such as the large-eddy simulations of Bardina *et al.*,[3] had clearly shown that frame rotation (Fig. 1) can act to either stabilize or destabilize homogeneous shear flow, depending on the ratio of the frame rotation rate to the shear rate. More recently, Salhi and Cambon[4] and Salhi[5] studied the case of homogeneous hydrodynamic shear in a rotating frame in greater detail focusing mostly on rapid distortion theory (RDT) analysis and DNS results. Brethouwer[6] has used a combination of analysis and numerical simulations to investigate the effect of frame rotation on the transport of a passive scalar in homogeneous shear flow. While studies such as these have helped to clarify the global features of homogeneous shear flow in a rotating frame, important details, such as long-time asymptotic states, and the details of the transition from the stable to the unstable regimes remain unclear.

Apart from experiments and DNS, considerable insight in the stability of rotated shear flows, can be gained through RDT. Under RDT the nonlinear effects resulting from turbulence-turbulence interactions are neglected in the governing equations. RDT is a closed theory for two-point correlations or spectra, but the one-point governing equations are, in general, not closed due to the nonlocality of the pressure fluctuations as explained by Townsend,[7] Hunt,[8] Savill,[9] Hunt and Carruthers,[10] and Cambon and Scott.[11] Simple cases of rapid deformation often admit closed-form solutions for individual Fourier coefficients. Even when such closed-form solutions are possible in spectral space, the integrals involved in forming the corresponding one-point statistics are often too complex to evaluate in closed form, and one is then forced to resort to numerical integration. The few cases where closed-form solutions can be obtained for one-point statistics, like the Reynolds stresses, offer valuable insight. For example, Rogers[12] was able to derive closed-form solutions for the spectra of homogeneous turbulence that is being sheared in a fixed frame. These solutions provide valuable insight in the distribution of energy in spectral space and also lead to estimates of the asymptotic behavior of one-point statistics, such as the Reynolds stresses, in the limit of large total shear.

In this study, we apply RDT to nonstratified homogeneous turbulence that is sheared in a frame which counter-rotates at a rate that exactly matches the rotation associated with the mean shear. This case relates to the classical test case of channel flow rotating about the spanwise direction, and it is also relevant for rotating free shear flow studied by Metais *et al.*[13] We develop closed-form solutions that are not limited to spectral quantities in Fourier space, but can be evaluated for one-point statistics such as the Reynolds stresses and the structure dimensionality tensor (see Kassinos and Rogers[14–16]). From these solutions the long time behavior of turbulence statistics such as the Reynolds stresses is studied in detail. Finally, the development of the structure of a passive scalar field with a constant mean scalar gradient is investigated, and some remarkable analogies are shown to exist between the present analysis and the case of shear in a fixed frame, studied by Rogers.[12]

[a]Also at the Institute of Environmental Research, National Observatory of Athens, Athens, Greece.
[b]Also at the Center for Turbulence Research, Stanford University/NASA-Ames, Stanford, California.

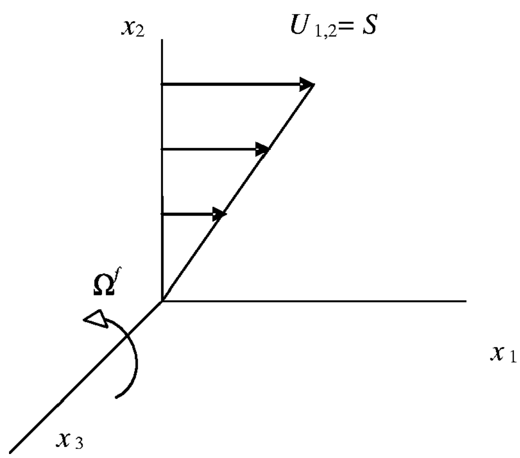

FIG. 1. Illustration of the general case for nonstratified homogeneous turbulence that is sheared in a rotating frame, which is examined here.

II. GOVERNING EQUATIONS

Under inviscid RDT, the transport equations for the fluctuating velocity components u_i become (Kassinos and Reynolds,[15,16] Brethouwer[6])

$$\frac{\partial u_i}{\partial t} + Sx_2\frac{\partial u_i}{\partial x_1} = -\delta_{i1}Su_2 - \frac{1}{\rho}\frac{\partial p}{\partial x_i} + \varepsilon_{ij3}2\Omega^f u_j, \tag{1}$$

where $S=dU_1/dx_2$ is the mean velocity gradient and Ω^f is the frame rotation rate (Fig. 1). Using the Rogallo[17] transformation we set

$$\xi_1 = x_1 - x_2St, \quad \xi_2 = x_2, \quad \xi_3 = x_3, \quad \tau = t \tag{2}$$

and (1) transforms to

$$\frac{\partial u_i}{\partial \tau} = -\delta_{i1}Su_2 - \frac{1}{\rho}\frac{\partial p}{\partial \xi_i} + \delta_{i2}S\tau\frac{\partial p}{\partial \xi_1} + \varepsilon_{ij3}2\Omega^f u_j. \tag{3}$$

Through (3), the Fourier transformed variables (denoted with $\hat{}$) evolve according to

$$\frac{d\hat{u}_i}{d\tau} = -\delta_{i1}S\hat{u}_2 + \frac{i}{\rho}\hat{p}(k_i - \delta_{i2}S\tau k_1) + \varepsilon_{ij3}2\Omega^f\hat{u}_j, \tag{4}$$

and after elimination of the pressure (using the continuity equation),

$$\frac{i}{\rho}\hat{p} = \frac{-k_1 2\Omega^f\hat{u}_2 + (k_2 - S\tau k_1)2\Omega^f\hat{u}_1 + 2k_1S\hat{u}_2}{k_1^2 + k_3^2 + (k_2 - S\tau k_1)^2}, \tag{5}$$

the system (4) is simplified to

$$\frac{d\hat{u}_1}{d\beta} = \frac{-k_1\eta\hat{u}_2 + (k_2 - k_1\beta)\eta\hat{u}_1 + 2k_1\hat{u}_2}{k_0^2 - 2k_1k_2\beta + k_1^2\beta^2}k_1 + (\eta - 1)\hat{u}_2,$$

$$\frac{d\hat{u}_2}{d\beta} = \frac{-k_1\eta\hat{u}_2 + (k_2 - k_1\beta)\eta\hat{u}_1 + 2k_1\hat{u}_2}{k_0^2 - 2k_1k_2\beta + k_1^2\beta^2}(k_2 - k_1\beta) - \eta\hat{u}_1, \tag{6}$$

$$\frac{d\hat{u}_3}{d\beta} = \frac{-k_1\eta\hat{u}_2 + (k_2 - k_1\beta)\eta\hat{u}_1 + 2k_1\hat{u}_2}{k_0^2 - 2k_1k_2\beta + k_1^2\beta^2}k_3,$$

where $k_0^2 = k_1^2 + k_2^2 + k_3^2$, $\beta = St$ (total shear) and $\eta = 2\Omega^f/S$.

Based on this general system, Salhi[5] has calculated complicated expressions in terms of the turbulent energy spectra E_{ii}, for a generalized η. In his analysis it is clear that the stability of the turbulent kinetic energy depends on the Bradshaw number $B=\eta(1-\eta)$ (Bradshaw[18]). More specifically, the unstable regime corresponds to positive values of B and it is characterized by an exponential energy growth (Brethouwer[6]). In this regime, it can be proven that quite simple 2D solutions using $k_1=0$ (i.e., independent of the x_1 direction), as described by Salhi,[5] represent well the stress field development and the exponential evolution of the turbulent kinetic energy with time. However, at the limits of the unstable regime for $B=0$, when either $\eta=0$ or $\eta=1$, the numerical results imply that the energy growth becomes linear with time. In these cases, it can be shown that the two-dimensional RDT (2D-RDT) approach, with $k_1=0$, drives turbulence to a different asymptotic behavior and results in a wrong estimation of the energy growth as $R_{nn}(\beta) \sim \beta^2$. Therefore, it is clear that for these two cases the 3D character of the turbulence can hardly be simplified. Rogers[12] has derived a 3D spectral solution for $\eta=0$ (the case where frame rotation is not present), from which he has approximated the long time asymptotic states for the stress components.

In the present study, we investigate the three-dimensional inviscid RDT (3D-RDT) solution for the evolution of an initially isotropic, nonstratified turbulence and compute the stresses $R_{ij}=\overline{u_iu_j}$ and the structure dimensionality tensor D_{ij} in the upper unstable limit for $\eta=1$, when the frame counter-rotates at a rotation rate that matches in magnitude that of the rotation associated with the mean shear. The structure dimensionality tensor D_{ij} is discussed in detail by Kassinos *et al.*[19] and gives information about the dimensionality of the turbulence. For example, if $D_{11}=0$, then the turbulence is independent of the x_1 axis; that is, it consists of very long structures aligned with the x_1 direction. The results of our analytical solution are compared with the exact inviscid RDT solution computed numerically using the particle representation model (PRM) developed by Kassinos and Reynolds,[14–16] as well as with the DNS performed by Brethouwer.[6]

III. DEVELOPMENT OF THE SPECTRAL SOLUTION

For $\eta=1$ the above system of equations (6) becomes

$$\frac{d\hat{u}_1}{d\beta} = \frac{k_1(k_2 - k_1\beta)\hat{u}_1 + k_1^2\hat{u}_2}{k_0^2 - 2k_1k_2\beta + k_1^2\beta^2},$$

$$\frac{d\hat{u}_2}{d\beta} = \frac{-(k_1^2 + k_3^2)\hat{u}_1 + k_1(k_2 - k_1\beta)\hat{u}_2}{k_0^2 - 2k_1k_2\beta + k_1^2\beta^2}, \tag{7}$$

$$\frac{d\hat{u}_3}{d\beta} = \frac{(k_2 - k_1\beta)k_3\hat{u}_1 + k_1k_3\hat{u}_2}{k_0^2 - 2k_1k_2\beta + k_1^2\beta^2},$$

from which we can show that

$$\hat{u}_1=\hat{u}_1^0+\frac{k_1}{k_3}\hat{u}_3-\frac{k_1}{k_3}\hat{u}_3^0, \quad \hat{u}_2=-\frac{k_1\hat{u}_1+k_3\hat{u}_3}{(k_2-k_1\beta)}, \quad \hat{u}_3=\hat{u}_3^0+\frac{k_3}{k_1}\hat{u}_1-\frac{k_3}{k_1}\hat{u}_1^0, \tag{8}$$

where the superscript 0, is used to denote an initial value. Combining the above equations (7) and (8), the final expressions for $\hat{u}_i(\beta)$ become

$$\hat{u}_1=\frac{\hat{u}_1^0(k_0^2-k_1k_2\beta)+\hat{u}_2^0k_1^2\beta}{k_0^2-2k_1k_2\beta+k_1^2\beta^2}, \quad \hat{u}_2=\frac{-(k_1^2+k_3^2)\beta\hat{u}_1^0+(k_0^2-k_1k_2\beta)\hat{u}_2^0}{k_0^2-2k_1k_2\beta+k_1^2\beta^2},$$

$$\hat{u}_3=\frac{-(k_1k_3\hat{u}_1^0-k_1^2\hat{u}_3^0)(k_0^2-2k_1k_2\beta+k_1^2\beta^2)-k_3(k_2-k_1\beta)\hat{u}_2^0k_0^2}{(k_1^2+k_3^2)(k_0^2-2k_1k_2\beta+k_1^2\beta^2)}-\frac{(k_3k_2\beta-k_1k_3\beta^2)(k_1k_3\hat{u}_3^0-k_3^2\hat{u}_1^0)}{(k_1^2+k_3^2)(k_0^2-2k_1k_2\beta+k_1^2\beta^2)}. \tag{9}$$

Using (9), the spectra $E_{ij}=\overline{\hat{u}_i\hat{u}_j^*}$ are calculated as

$$E_{11}=\frac{E_{11}^0(k_0^2-k_1k_2\beta)^2+E_{22}^0k_1^4\beta^2+(k_0^2k_1^2\beta-k_1^3k_2\beta^2)(E_{12}^0+E_{21}^0)}{(k_0^2-2k_1k_2\beta+k_1^2\beta^2)^2},$$

$$E_{22}=\frac{(k_1^2+k_3^2)^2\beta^2E_{11}^0+(k_0^2-k_1k_2\beta)^2E_{22}^0-(k_1^2+k_3^2)(k_0^2\beta-k_1k_2\beta^2)(E_{12}^0+E_{21}^0)}{(k_0^2-2k_1k_2\beta+k_1^2\beta^2)^2},$$

$$E_{12}=\frac{-(k_1^2\beta+k_3^2\beta)(k_0^2-k_1k_2\beta)E_{11}^0+\beta(k_0^2k_1^2-k_1^3k_2\beta)E_{22}^0}{(k_0^2-2k_1k_2\beta+k_1^2\beta^2)^2}+\frac{(k_0^2-k_1k_2\beta)^2E_{12}^0-\beta^2(k_1^4+k_1^2k_3^2)E_{21}^0}{(k_0^2-2k_1k_2\beta+k_1^2\beta^2)^2}, \tag{10}$$

$$\begin{aligned}E_{33}=&\frac{(-k_1k_3k_0^2+(2k_1^2k_2k_3+k_3^3k_2)\beta-(k_1k_3^3+k_1^3k_3)\beta^2)^2}{(k_1^2+k_3^2)^2(k_0^2-2k_1k_2\beta+k_1^2\beta^2)^2}E_{11}^0+\frac{(-k_2k_3k_0^2+k_1k_3k_0^2\beta)^2}{(k_1^2+k_3^2)^2(k_0^2-2k_1k_2\beta+k_1^2\beta^2)^2}E_{22}^0\\
&+\frac{(k_1^2k_0^2-(k_1k_2k_3^2+2k_1^3k_2)\beta+(k_1^2k_3^2+k_1^4)\beta^2)^2}{(k_1^2+k_3^2)^2(k_0^2-2k_1k_2\beta+k_1^2\beta^2)^2}E_{33}^0\\
&+\frac{(-k_1k_3k_0^2+(2k_1^2k_2k_3+k_3^3k_2)\beta-(k_1k_3^3+k_1^3k_3)\beta^2)(-k_2k_3k_0^2+k_1k_3k_0^2\beta)}{(k_1^2+k_3^2)^2(k_0^2-2k_1k_2\beta+k_1^2\beta^2)^2}(E_{12}^0+E_{21}^0)\\
&+\frac{(-k_2k_3k_0^2+k_1k_3k_0^2\beta)(k_1^2k_0^2-(k_1k_2k_3^2+2k_1^3k_2)\beta+(k_1^2k_3^2+k_1^4)\beta^2)}{(k_1^2+k_3^2)^2(k_0^2-2k_1k_2\beta+k_1^2\beta^2)^2}(E_{23}^0+E_{32}^0)\\
&+[(2k_1^2k_2k_3+k_3^3k_2)\beta-k_1k_3k_0^2-(k_1k_3^3+k_1^3k_3)\beta^2]\times\frac{k_1^2k_0^2-(k_1k_2k_3^2+2k_1^3k_2)\beta+(k_1^2k_3^2+k_1^4)\beta^2}{(k_1^2+k_3^2)^2(k_0^2-2k_1k_2\beta+k_1^2\beta^2)^2}(E_{13}^0+E_{31}^0).\end{aligned}$$

From the numerical integration of Eqs. (10) for the calculation of the stress components $R_{ij}=\int_{\mathbf{k}}E_{ij}d^3\mathbf{k}$, or the equivalent PRM results (Fig. 2), it turns out that, for large β, the kinetic energy growth tends to the linear form

$$R_{ii}(\beta)=2R_{22}(\beta)=2R_{33}(\beta)=q_0^2\beta/2, \tag{11}$$

where $q_0^2=R_{ii}^0$ is twice the initial value of the turbulent kinetic energy. We must underline also, that the numerical results imply an equality between the stresses and the structure dimensionality tensor components [see Eq. (16)], $R_{ij}=D_{ij}$. As discussed later, we have proven this equality between the one-point tensors (in physical space), but it should be noted that the corresponding spectral expressions in Fourier space are not equal.

In the rotating frame, if $k_1=0$ initially, it remains so. That is, initially 2D-3C, which is independent of the streamwise direction remains 2D as the flow evolves. In this case formulas (9) and (10) simplify to

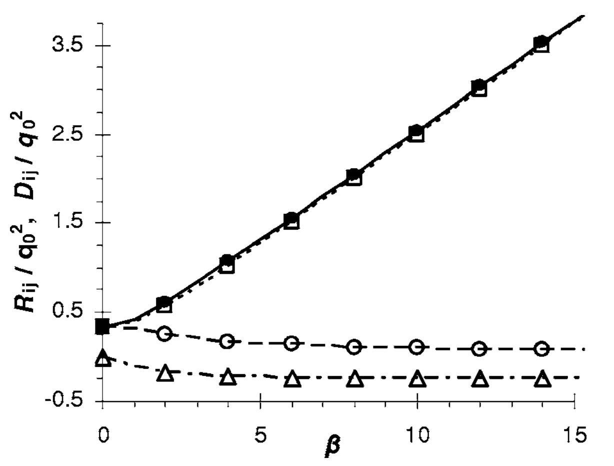

FIG. 2. Comparison between the evolution of the stress and the structure dimensionality tensor components: 11 (— —; ○), 22 (—; ●), 33 (---; □), and 12 (–·–; △) calculated from the analytical RDT solution presented here (lines) and the exact 3D-PRM numerical solution (symbols).

$$\hat{u}_1 = \hat{u}_1^0, \quad \hat{u}_2 = \hat{u}_2^0 - \frac{k_3^2\beta}{k_0^2}\hat{u}_1^0,$$

$$\hat{u}_3 = \hat{u}_3^0 + \frac{k_3 k_2 \beta}{k_0^2}\hat{u}_1^0, \quad E_{11}(\beta) = E_{11}^0,$$

$$E_{22}(\beta) = \frac{k_3^4\beta^2 E_{11}^0 + k_0^4 E_{22}^0 - k_3^2 k_0^2 \beta (E_{12}^0 + E_{21}^0)}{k_0^4}, \tag{12}$$

$$E_{12} = -\frac{k_3^2 \beta E_{11}^0}{k_0^2} + E_{12}^0,$$

$$E_{33}(\beta) = \frac{k_2^2}{k_3^2}E_{22}^0 + \frac{k_3^2 k_2^2 \beta^2}{k_0^4}E_{11}^0 - \frac{k_2^2\beta}{k_0^2}(E_{12}^0 + E_{21}^0)$$
$$= E_{33}^0 + \frac{k_2^2 k_3^2 \beta^2}{k_0^4}E_{11}^0 + \frac{k_2 k_3 \beta}{k_0^2}(E_{13}^0 + E_{31}^0).$$

While the integration of the 2D equations (12) leading to the components of the Reynolds stress and dimensionality tensors is straightforward, it unfortunately gives a $R_{nn}(\beta) \sim \beta^2$ behavior, which does not agree with the linear behavior of the 3D-PRM numerical results (11). Thus, preserving the 3D character of the turbulence is important for the correct estimation of the one-point statistics.

IV. ANALYTICAL CALCULATION OF THE STRESSES STARTING WITH AN ISOTROPIC SPECTRUM

In this section, we present the analytical solution for R_{ij}/q_0^2 starting with a 3D initially isotropic energy spectrum of the form

$$E_{ij}^0 = \frac{E(k_0)}{4\pi k_0^2}\left(\delta_{ij} - \frac{k_i k_j}{k_0^2}\right) \tag{13}$$

for $i=1,2,3$ and $j=1,2,3$. The initial turbulent kinetic energy spectrum $E(k_0)$ satisfies

$$\int_{k_0=0}^{\infty} E(k_0)dk_0 = \frac{q_0^2}{2} = \frac{R_{ii}^0}{2}. \tag{14}$$

For the derivation of both the stresses and the structure dimensionality tensor components, we analytically integrate the spectra given by Eqs. (10). The integrations are carried out in spherical coordinates where $k_1 = k_0 \cos\alpha$, $k_2 = k_0 \sin\alpha \sin\varphi$, $k_3 = k_0 \sin\alpha \cos\varphi$, $d^3k_0 = k_0^2 \sin\alpha dk_0 d\alpha d\varphi$, with $0 \leqslant \alpha \leqslant \pi$ and $0 \leqslant \varphi \leqslant 2\pi$ (due to symmetries the above limits can be reduced either to $0 \leqslant \alpha \leqslant \pi$ and $0 \leqslant \varphi \leqslant \pi/2$, or to $0 \leqslant \alpha \leqslant \pi/2$ and $0 \leqslant \varphi \leqslant 2\pi$). In this coordinate system, the dimensionless stresses (divided by twice the initial kinetic energy) are given by the following relations:

$$\frac{R_{11}}{q_0^2} = \frac{1}{8\pi}\int_0^{\pi}\int_0^{2\pi} \frac{\sin^2\alpha - 2\beta\cos\alpha\sin\alpha\sin\varphi + (\cos^2\alpha\sin^2\alpha\sin^2\varphi + \cos^4\alpha)\beta^2}{(1 - 2\beta\cos\alpha\sin\alpha\sin\varphi + \beta^2\cos^2\alpha)^2}\sin\alpha d\varphi d\alpha,$$

$$\frac{R_{22}}{q_0^2} = \frac{1}{8\pi}\int_0^{\pi}\int_0^{2\pi} \frac{(\cos^2\alpha\sin^2\varphi + \cos^2\varphi)(1 + \beta^2\cos^2\varphi\sin^2\alpha)\sin\alpha}{(1 - 2\beta\cos\alpha\sin\alpha\sin\varphi + \beta^2\cos^2\alpha)^2}d\varphi d\alpha, \tag{15}$$

$$\frac{R_{33}}{q_0^2} = \frac{1}{8\pi}\int_0^{\pi}\int_0^{2\pi}[48 + 87\beta^2 + 28\beta^4 - 32\sin^2\alpha\cos 2\varphi + (4\beta^4 - 19\beta^2)\cos 4\alpha + 4\cos 2\alpha(4 + 15\beta^2 + 8\beta^4$$
$$- 14\beta^3\sin 2\alpha\sin\varphi) + (8\beta^4 - 24\beta^2)\sin^2 2\alpha\cos 2\varphi - (72\beta^3 + 128\beta)\sin 2\alpha\sin\varphi - 32\beta^3\cos\alpha\sin^3\alpha\sin 3\varphi$$
$$- 8\beta^2\sin^4\alpha\cos 4\varphi] \times \frac{\sin\alpha}{64(1 - 2\beta\cos\alpha\sin\alpha\sin\varphi + \beta^2\cos^2\alpha)^2}d\varphi d\alpha,$$

$$\frac{R_{12}}{q_0^2} = \frac{1}{8\pi}\int_0^{\pi}\int_0^{2\pi} \frac{-\cos\alpha\sin\alpha\sin\varphi + \beta(\cos^2\alpha - \sin^2\alpha\cos^2\varphi) + \beta^2(\sin^3\alpha\cos^2\varphi\sin\varphi)}{(1 - 2\beta\cos\alpha\sin\alpha\sin\varphi + \beta^2\cos^2\alpha)^2}\sin\alpha d\varphi d\alpha.$$

The components of the structure dimensionality tensor D_{ij} (Kassinos[19]) are calculated through

$$D_{ij}(\beta) = \int_{\mathbf{k}} E_{ii}(\mathbf{k},\beta)\frac{(k_i - \delta_{i2}\beta k_1)(k_j - \delta_{j2}\beta k_1)}{k^2}d^3\mathbf{k}, \tag{16}$$

where $\mathbf{k}$ is the wave number vector, with magnitude $k = \sqrt{k_0^2 - 2k_1k_2\beta + k_1^2\beta^2}$. Despite the fact that the spectral integrands in Eq. (16) are not equal to the respective ones in Eqs. (15), we have proven (however this requires some effort and it is not shown here) that the integrations lead to the same results in physical space. More specifically, one can show that the analytical integrations of component differences, for example, if we integrate the difference of the spectral integrand corresponding to R_{11} in (15) minus the respective spectral integrand corresponding to D_{11} in (16), we find a vanishing result. Therefore as pointed out previously, $D_{ij} = R_{ij}$ at all values of total shear St. After the analytical integration of (15), which is presented in the Appendix, the stresses $R_{ij}(\beta)/q_0^2$, are given by

$$\frac{R_{11}(\beta)}{q_0^2}=\frac{D_{11}(\beta)}{q_0^2}=\frac{-E_1(\beta)+(\beta^2+1-2i\beta)E_2(\beta)}{4\beta(\beta-2i)\sqrt{\beta(\beta+2i)}},$$

$$\begin{aligned}\frac{R_{22}(\beta)}{q_0^2}&=\frac{D_{22}(\beta)}{q_0^2}=\frac{R_{11}(\beta)}{q_0^2}-\beta\frac{R_{12}(\beta)}{q_0^2}\\&=\frac{D_{11}(\beta)}{q_0^2}-\beta\frac{D_{12}(\beta)}{q_0^2},\end{aligned}$$

$$\begin{aligned}R_{33}(\beta)/q_0^2&=\frac{1}{4}+\frac{\beta^2+1}{8}\\&\quad+\frac{(\beta^2+1)(2-i\beta)E_1(\beta)-2(\beta^2+1)E_2(\beta)}{8\beta\sqrt{-\beta(\beta+2i)}},\end{aligned} \tag{17}$$

$$\begin{aligned}\frac{R_{12}(\beta)}{q_0^2}&=\frac{D_{12}(\beta)}{q_0^2}\\&=\frac{-(\beta^2+1)}{8\beta}+\frac{i\beta(3+\beta^2)E_1(\beta)}{8\beta(\beta-2i)\sqrt{-\beta(\beta+2i)}}\\&\quad+\frac{2(\beta-i)^2E_2(\beta)}{8\beta(\beta-2i)\sqrt{-\beta(\beta+2i)}}.\end{aligned}$$

In the above, the expressions $E_1(\beta)$ and $E_2(\beta)$ are functions of elliptic integrals of the first and the second kind as shown in the Appendix.

It has to be pointed out that $R_{11}(\eta=1,\beta)/q_0^2$ in (17) equals (for any value of the total shear β) the normal stress component $R_{22}(\eta=0,\beta)/q_0^2$, which is obtained when one integrates the corresponding spectral expression given by Rogers[12] for the case with $\eta=0$. We proved this equality by taking the respective spectral solution and showing that the integrations lead to the same results in physical space. Therefore, $R_{11}(\eta=1,\beta)/q_0^2$, Eq. (17), is the analytical solution (not known up to now) for $R_{22}(\eta=0,\beta)/q_0^2$ as well, when there is only shear without any rotation of the frame. For the remaining stress components, however, no such similarities exist between the two different cases.

Taking the sum of Eqs. (17) the turbulent kinetic energy ($\times 2$) evolves as

$$\begin{aligned}R_{ii}(\beta)/q_0^2&=\frac{1}{4}+\frac{\beta^2+1}{4}+\frac{(\beta^3+4\beta)E_1(\beta)}{4(\beta-2i)\sqrt{\beta(\beta+2i)}}\\&\quad-\frac{(i\beta^2+\beta+2i)E_2(\beta)}{2(\beta-2i)\sqrt{\beta(\beta+2i)}}.\end{aligned} \tag{18}$$

Asymptotic behavior of the stresses: From the investigation of the limits of the above analytical solutions, it follows that, in the limit of large total shear, $R_{12}(\beta)/q_0^2$ reaches the fixed value of -0.25 and hence, the sum of the normal stresses evolves as 0.5β. The asymptotic behavior of all the stress components is given below:

$$\begin{aligned}&\frac{R_{11}}{q_0^2}\to\frac{\ln(4\beta)}{4\beta},\quad \frac{R_{22}}{q_0^2}\to 0.25\beta,\\&\frac{R_{33}}{q_0^2}\to 0.25\beta,\quad \frac{R_{12}}{q_0^2}\to -0.25.\end{aligned} \tag{19}$$

The above limits (19) are reached relatively fast, for $\beta\approx 5$, within an accuracy of 1% in the case of R_{11} and 5% for R_{22}, R_{33} and R_{12}. For the sake of simplicity, a very accurate approximation may be derived for R_{12} in (17)

$$\frac{R_{12}(\beta)}{q_0^2}=-\frac{0.25\beta}{\sqrt{3.5+\beta^2}}, \tag{20}$$

and as a result, the turbulent kinetic energy evolution ($\times 2$) can be approximated by

$$\frac{R_{nn}(\beta)}{q_0^2}=\frac{\sqrt{3.5+\beta^2}+2-\sqrt{3.5}}{2}. \tag{21}$$

The results given in Eqs. (20) and (21) do not differ, for any value of β, by more than 0.3% from the exact solutions given in (17).

As shown above, the asymptotic state for R_{11} equals the respective one reported by Rogers[12] for R_{22}, for the case without any frame rotation. For the remaining stress components there are no such similarities. However, one can note that in both cases, the shear stress tends to a constant value, causing the turbulent kinetic energy to evolve linearly with time. In the case with $\eta=0$, however, the shear stress tends to a larger asymptotic value ($-\ln 2$), and this results into a faster energy growth compared to the case investigated here. This is also supported by the studies of Bardina *et al.*,[3] Salhi and Cambon,[4] and Brethouwer.[6]

Looking at the normalized stresses $r_{ij}=R_{ij}/R_{ii}$ and the normalized structure dimensionality components $d_{ij}=D_{ij}/D_{ii}$ we can gather information on the anisotropy of turbulence. The asymptotic states of the normalized tensor components corresponding to (19) reveal a two-dimensional, two-component state (Kassinos *et al.*[19]) with $d_{11}=r_{11}\to 0$, $d_{22}=r_{22}\to 1/2$ and $d_{33}=r_{33}\to 1/2$. The fact that this state is reached relatively quickly (for $\beta\approx 5$) would seem to suggest that a simplified analysis based on an initially 2D state with $k_1=0$ would provide a good approximation to the exact evolution of the tensor components. In fact, as noted previously, such an approximation fails to capture the correct turbulent kinetic energy growth, suggesting that in this case the 3D character of the turbulence at early times plays a key role in determining the evolution at later times (this holds true also for the case without frame rotation).

V. COMPARISONS WITH PRM NUMERICAL RESULTS AND DNS

The stresses calculated analytically, through Eqs. (17), are identical to the exact inviscid RDT solution computed numerically using the 3D-PRM, as shown in Fig. 2. In Fig. 3 we illustrate another comparison, between the energy growth calculated (a) through the analysis presented here and (b) from the DNS data of Brethouwer.[6] Although there is a dif-

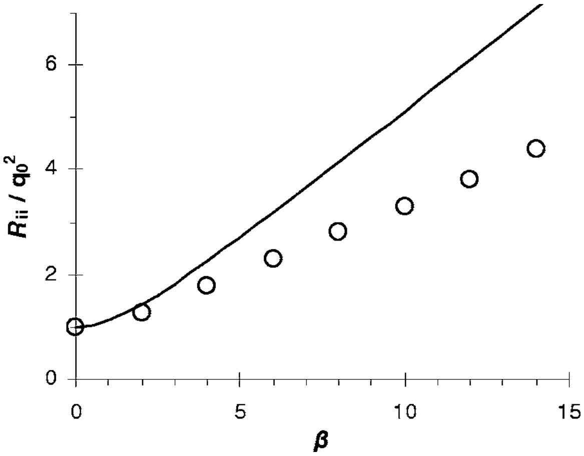

FIG. 3. Comparison between the energy growth calculated from the present analysis (—) and the DNS data (○) from Brethouwer (Ref. 6).

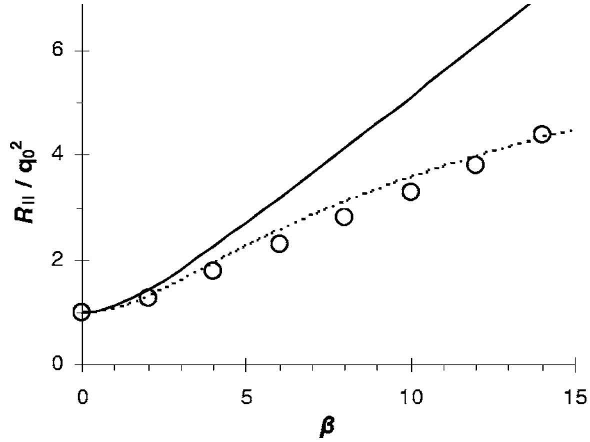

FIG. 5. Comparison between the evolution of the turbulent kinetic energy given by the inviscid RDT analysis (—), the DNS data (○) from Brethouwer (Ref. 6), and the solution of Eq. (35) (- - -) for $\overline{2\varepsilon(\beta)/SR_{ii}(\beta)}=0.066$.

ference in the rate of the energy growth, its linearity with β is clear in both cases. The higher growth rates calculated through the analytical RDT equations could be mainly attributed to the absence of the viscosity, as it is argued below; in fact numerical simulations of viscous RDT (no nonlinear contributions) presented by Brethouwer[6] reveal a very close agreement with the DNS data (including the nonlinear terms).

As shown in Fig. 4, the observed difference in the energy is mainly due to the stress components R_{22} and R_{33}. Nevertheless, there is a very good agreement for the values of R_{11} and R_{12} from the two data sets. The last remarks can be used in order to achieve a rough quantitative estimation of how viscosity creates the energy difference. This can be done through the governing equation for the turbulent kinetic energy ($\times 2$),

$$\frac{\partial R_{ii}(\beta)}{\partial\beta} = -2R_{12}(\beta) - \frac{2\varepsilon(\beta)}{S}, \tag{22}$$

which can be rewritten as

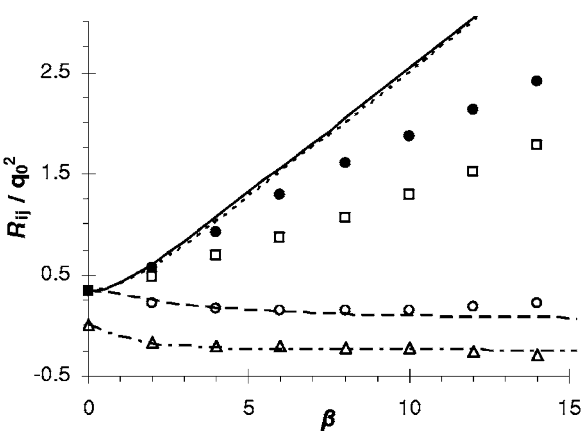

FIG. 4. Comparison between the evolution of the stress components: 11 (— —; ○), 22 (—; ●), 33 (---; □), and 12 (-·-; △) calculated from the RDT analysis presented here (lines) and the DNS data (symbols) from Brethouwer (Ref. 6).

$$\frac{\partial R_{ii}(\beta)/q_0^2}{\partial\beta} = \frac{-2R_{12}(\beta)}{q_0^2} - \frac{2\varepsilon(\beta)}{SR_{ii}(\beta)}\frac{R_{ii}(\beta)}{q_0^2}, \tag{23}$$

where $\varepsilon(\beta)$ is the dissipation of the turbulent kinetic energy. Using the DNS results of Brethouwer,[6] for $\eta=1$, we calculated the ratio $2\varepsilon(\beta)/SR_{ii}(\beta)$ for values of β between 0 and 8, to be in the range 0.056–0.077. Also the linear viscous RDT numerical simulations, by the same author, give approximately the same values for this ratio. Taking into account the relatively small variation of the above term, we present numerical results of the following equation, substituting the above term by an average value of 0.066,

$$\frac{\partial R_{ii}(\beta)/q_0^2}{\partial\beta} = \frac{-2R_{12}(\beta)}{q_0^2} - \overline{\left(\frac{2\varepsilon(\beta)}{SR_{ii}(\beta)}\right)}\frac{R_{ii}(\beta)}{q_0^2}. \tag{24}$$

From the comparison of the solution of (24) with the DNS data in Fig. 5, it follows that the viscosity itself explains most of the differences in the turbulent kinetic energy, while it is implied that the role of the nonlinearity is less important for such large values of SK/ε, for the specific value of $\eta=1$. A similar picture appears from the comparison between the numerical results from linear and nonlinear numerical simulations presented by Brethouwer.[6] In his Figs. 13 and 14 it is apparent that the differences between the viscous RDT and the DNS are small regarding the shear stress and the turbulent kinetic energy evolution when $\eta=1$.

In order to achieve a better picture on the role of the nonlinearity on the present application we present in Fig. 6 the rapid part of the pressure strain, which in the case of shear $S=\mathrm{d}U_1/\mathrm{d}x_2$ is

$$\Pi_{ij}^r = 2S(M_{i21j} + M_{j21i}), \tag{25}$$

with M_{ipqj} given by

$$M_{pqij}(\beta) = \int_{\mathbf{k}} E_{ip}(\mathbf{k},\beta)\frac{(k_q - \delta_{q2}\beta k_1)(k_j - \delta_{j2}\beta k_1)}{k^2} d^3\mathbf{k}. \tag{26}$$

The comparison with the respective Π_{ij}^r from the DNS reveals a close agreement up to a value of the total shear equal

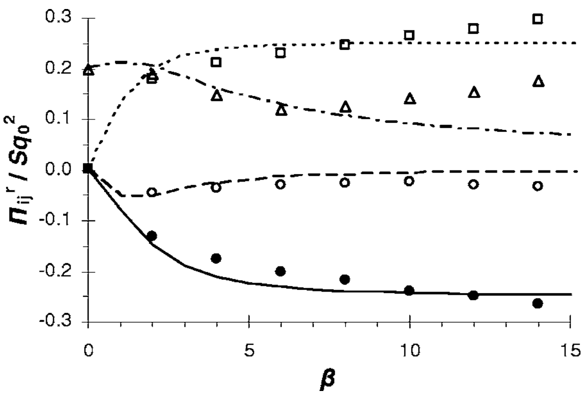

FIG. 6. Comparison of the rapid pressure strain components: 11 (— —; ○), 22 (—; ●), 33 (---; □), and 12 (–·–; △) calculated from the analysis presented here (lines) and the DNS data (symbols) from Brethouwer (Ref. 6).

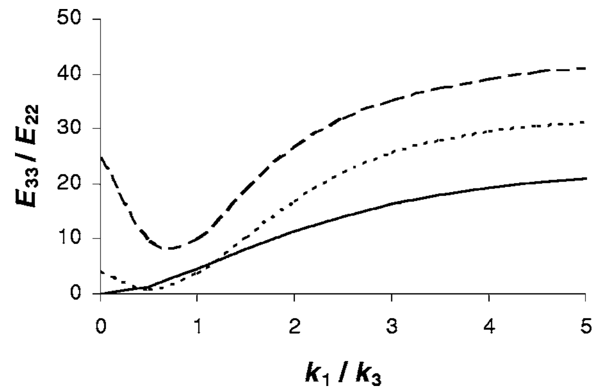

FIG. 8. The ratio of the spectra E_{33} divided by E_{22} as a function of k_1/k_3 for $\beta=2$. Lines correspond to different values of $k_2/k_3=0$ (— —), 2 (---), and 5 (—).

to 8. For larger times the DNS values start to deviate gradually from the asymptotic behavior of the inviscid RDT, which has been estimated in this study as

$$\frac{\Pi_{11}^r}{Sq_0^2} \sim -1/\beta^2 \to 0, \quad \frac{\Pi_{22}^r}{Sq_0^2} \to -0.25,$$
$$\frac{\Pi_{33}^r}{Sq_0^2} \to 0.25, \quad \frac{\Pi_{12}^r}{Sq_0^2} \sim \ln \beta/\beta \to 0. \tag{27}$$

The respective slow parts of the pressure strain, from the DNS of Brethouwer,[6] remain small compared to the rapid parts at least up to β equal to 8 and thus they do not affect markedly the presented results. However, for large enough values of the total shear the nonlinearity could drive the DNS to deviate significantly from RDT.

Figure 7 displays the evolution of the normalized stresses $r_{ij}=R_{ij}/R_{ii}$, which represent the energy share between the different components of the stress tensor. Our results compare favorably with the DNS with the exception that the DNS (as well as the respective viscous RDT simulations of Brethouwer[6]) imply a slightly different distribution of the kinetic energy between R_{22} and R_{33}. Specifically, R_{33} becomes smaller than R_{22}, contrary to inviscid RDT theory

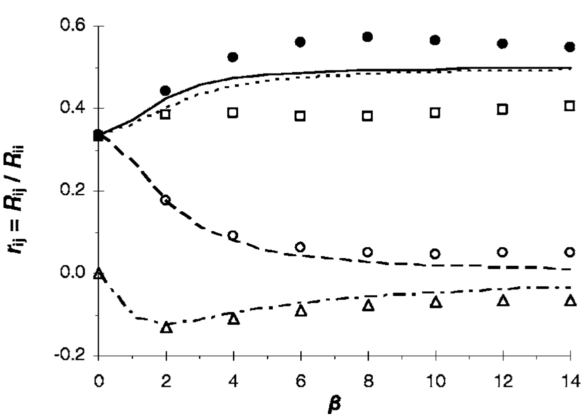

FIG. 7. Comparison between the normalized stresses: 11 (— —; ○), 22 (—; ●), 33 (---; □), and 12 (–·–; △) calculated from the analysis presented here (lines) and the DNS data (symbols) from Brethouwer (Ref. 6).

which predicts an equal partition of turbulent energy between them, $R_{22}=R_{33}$. One possible explanation is that, as shown in Fig. 8, for any given value of the wave numbers k_2 and k_3 the spectrum E_{33} exceeds E_{22} as k_1 increases. As a result, R_{33} component has markedly more energy at high wave numbers compared to R_{22} and thus it is more sensitive to viscous dissipation.

VI. FLUXES OF A PASSIVE SCALAR WITH A CONSTANT MEAN GRADIENT

The scalar fluctuations θ, of a passive scalar Θ, with a constant mean gradient $G_i=\partial\bar{\Theta}/\partial x_i$, are governed by (Rogers[12] and Brethouwer[6])

$$\frac{\partial\theta}{\partial t} + Sx_2\theta_{,1} + u_jG_j + (\theta u_j)_{,j} = \gamma\theta_{,jj}, \tag{28}$$

where γ is the molecular diffusivity. Note that in the previous expression the frame rotation rate is not present. However, the effect of the rotation is encountered through its influence on the velocity components. By neglecting the nonlinear term $(\theta u_j)_{,j}$, the above equation yields the linear form

$$\frac{\partial\theta}{\partial t} + Sx_2\theta_{,1} + u_jG_j = \gamma\theta_{,jj}. \tag{29}$$

We study two cases for the mean scalar gradient here: $\overline{\Theta}_1 = G_1x_1$ and $\overline{\Theta}_2 = G_2x_2$. The corresponding scalar fluctuations will be denoted as θ_1 and θ_2, respectively. Thus the linear equations to be solved are

$$\frac{\partial\theta_1}{\partial t} + Sx_2\theta_{1,1} + u_1G_1 = \gamma\theta_{1,jj},$$
$$\frac{\partial\theta_2}{\partial t} + Sx_2\theta_{2,1} + u_2G_2 = \gamma\theta_{2,jj}, \tag{30}$$

which after the Rogallo transformation, for Prandtl number equal to 1, $\mathrm{Pr}=\nu/\gamma=1$, and for an inviscid fluid (which implies that $\gamma=0$) become

$$\frac{\partial\theta_1}{\partial\tau}+u_1G_1=0,\quad \frac{\partial\theta_2}{\partial\tau}+u_2G_2=0. \tag{31}$$

Using Eqs. (9), the evolution of the Fourier transformed variables is given by

$$S\frac{\partial\hat{\theta}_1}{\partial\beta}=\frac{-G_1\hat{u}_1^0(k_0^2-k_1k_2\beta)-G_1\hat{u}_2^0k_1^2\beta}{k_0^2-2k_1k_2\beta+k_1^2\beta^2},$$
$$S\frac{\partial\hat{\theta}_2}{\partial\beta}=\frac{G_2\hat{u}_1^0(k_1^2+k_3^2)\beta-G_2\hat{u}_2^0(k_0^2-k_1k_2\beta)}{k_0^2-2k_1k_2\beta+k_1^2\beta^2}. \tag{32}$$

Performing the integrations, we obtain the solution for the evolution of $\hat{\theta}_1$ and $\hat{\theta}_2$

$$S\hat{\theta}_1=S\hat{\theta}_1^0-G_1\hat{u}_1^0\frac{\sqrt{k_1^2+k_3^2}}{k_1}\left(\arctan\frac{\beta k_1-k_2}{\sqrt{k_1^2+k_3^2}}+\arctan\frac{k_2}{\sqrt{k_1^2+k_3^2}}\right)-G_1\hat{u}_1^0\frac{k_2}{2k_1}\ln\left(\frac{k_0^2}{k_0^2-2\beta k_1k_2+\beta^2k_1^2}\right)$$
$$-G_1\hat{u}_2^0\frac{k_2}{\sqrt{k_1^2+k_3^2}}\left(\arctan\frac{\beta k_1-k_2}{\sqrt{k_1^2+k_3^2}}+\arctan\frac{k_2}{\sqrt{k_1^2+k_3^2}}\right)+G_1\hat{u}_2^0\frac{1}{2}\ln\left(\frac{k_0^2}{k_0^2-2\beta k_1k_2+\beta^2k_1^2}\right),$$
$$S\hat{\theta}_2=S\hat{\theta}_2^0-G_2\hat{u}_2^0\frac{\sqrt{k_1^2+k_3^2}}{k_1}\left(\arctan\frac{\beta k_1-k_2}{\sqrt{k_1^2+k_3^2}}+\arctan\frac{k_2}{\sqrt{k_1^2+k_3^2}}\right)-G_2\hat{u}_2^0\frac{k_2}{2k_1}\ln\left(\frac{k_0^2}{k_0^2-2\beta k_1k_2+\beta^2k_1^2}\right)$$
$$+G_2\hat{u}_1^0\frac{k_2\sqrt{k_1^2+k_3^2}}{k_1^2}\left(\arctan\frac{\beta k_1-k_2}{\sqrt{k_1^2+k_3^2}}+\arctan\frac{k_2}{\sqrt{k_1^2+k_3^2}}\right)-G_2\hat{u}_1^0\frac{k_1^2+k_3^2}{2k_1^2}\ln\left(\frac{k_0^2}{k_0^2-2\beta k_1k_2+\beta^2k_1^2}\right). \tag{33}$$

Combining the above with the solutions for the velocity components [Eqs. (9)] and considering zero scalar fluxes initially $\overline{u_i^0\theta_j^0}=0$, we derive the spectra $\mathbf{\Phi}_{jj}(\beta)=\hat{\theta}_j(\beta)\hat{\theta}_j^*(\beta)$, and the cross-spectra $\mathbf{\Phi}_j^i(\beta)=\hat{u}_i(\beta)\hat{\theta}_j^*(\beta)$, for the passive scalar, where the index $i=1,2$ refers to the velocity component, and $j=1,2$ to the choice of the scalar gradient (no summation implied by the repeated indexes). The respective expressions for the cross-spectra with respect to u_3 have been omitted, since after their integration over all the wave numbers, the respective fluxes result zero.

In the case of $\hat{\theta}_1$ the spectra become

$$\frac{S\Phi_1^1}{G_1}=-\frac{E_{11}^0(k_0^2-k_1k_2\beta)+E_{12}^0k_1^2\beta}{k_0^2-2\beta k_1k_2+\beta^2k_1^2}A_1(\mathbf{k},\beta)-\frac{E_{22}^0k_1^2\beta+E_{21}^0(k_0^2-k_1k_2\beta)}{k_0^2-2\beta k_1k_2+\beta^2k_1^2}A_2(\mathbf{k},\beta),$$

$$\frac{S\Phi_1^2}{G_1}=\frac{E_{11}^0(k_1^2+k_3^2)\beta-E_{12}^0(k_0^2-k_1k_2\beta)}{k_0^2-2\beta k_1k_2+\beta^2k_1^2}A_1(\mathbf{k},\beta)-\frac{E_{22}^0(k_0^2-k_1k_2\beta)-E_{21}^0(k_1^2+k_3^2)\beta}{k_0^2-2\beta k_1k_2+\beta^2k_1^2}A_2(\mathbf{k},\beta), \tag{34}$$

$$\frac{S^2\Phi_{11}}{G_1^2}-\frac{S^2\Phi_{11}^0}{G_1^2}=E_{11}^0A_1(\mathbf{k},\beta)^2+E_{22}^0A_2(\mathbf{k},\beta)^2+(E_{12}^0+E_{21}^0)A_1(\mathbf{k},\beta)A_2(\mathbf{k},\beta),$$

while in the case of $\hat{\theta}_2$ we find

$$\frac{S\Phi_2^1}{G_2}=\frac{E_{11}^0(k_0^2-k_1k_2\beta)+E_{21}^0k_1^2\beta}{(k_0^2-2k_1k_2\beta+k_1^2\beta^2)}A_3(\mathbf{k},\beta)-\frac{E_{22}^0k_1^2\beta+E_{12}^0(k_0^2-k_1k_2\beta)}{(k_0^2-2k_1k_2\beta+k_1^2\beta^2)}A_1(\mathbf{k},\beta),$$

$$\frac{S\Phi_2^2}{G_2}=\frac{-(k_1^2+k_3^2)\beta E_{11}^0+(k_0^2-k_1k_2\beta)E_{12}^0}{k_0^2-2k_1k_2\beta+k_1^2\beta^2}A_3(\mathbf{k},\beta)+\frac{-(k_0^2-k_1k_2\beta)E_{22}^0+(k_1^2+k_3^2)\beta E_{21}^0}{k_0^2-2k_1k_2\beta+k_1^2\beta^2}A_1(\mathbf{k},\beta), \tag{35}$$

$$\frac{S^2\Phi_{22}}{G_2^2}-\frac{S^2\Phi_{22}^0}{G_2^2}=E_{11}^0A_3(\mathbf{k},\beta)^2+E_{22}^0A_1(\mathbf{k},\beta)^2-(E_{12}^0+E_{21}^0)A_1(\mathbf{k},\beta)A_3(\mathbf{k},\beta),$$

where the expressions $A_1(\mathbf{k},\beta)$, $A_2(\mathbf{k},\beta)$, and $A_3(\mathbf{k},\beta)$ are given by

$$A_1(\mathbf{k},\beta)=\frac{\sqrt{k_1^2+k_3^2}}{k_1}\left(\arctan\frac{\beta k_1-k_2}{\sqrt{k_1^2+k_3^2}}+\arctan\frac{k_2}{\sqrt{k_1^2+k_3^2}}\right)+\frac{k_2}{2k_1}\ln\left(\frac{k_0^2}{k_0^2-2\beta k_1k_2+\beta^2k_1^2}\right),$$

$$A_2(\mathbf{k},\beta)=\frac{k_2}{\sqrt{k_1^2+k_3^2}}\left(\arctan\frac{\beta k_1-k_2}{\sqrt{k_1^2+k_3^2}}+\arctan\frac{k_2}{\sqrt{k_1^2+k_3^2}}\right)-\frac{1}{2}\ln\left(\frac{k_0^2}{k_0^2-2\beta k_1k_2+\beta^2k_1^2}\right), \tag{36}$$

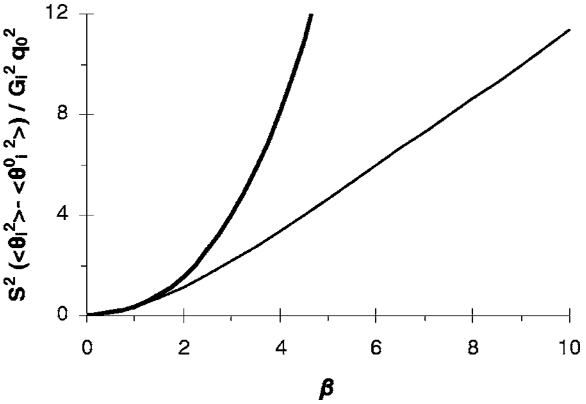

FIG. 9. Time development of the scalar fluctuation intensities: $S^2(\overline{\theta_1^2}-\overline{\theta_1^0\theta_1^0})/G_1^2q_0^2\sim\beta$ (thin line) and $S^2(\overline{\theta_2^2}-\overline{\theta_2^0\theta_2^0})/G_2^2q_0^2\sim\beta^3$ (thick line).

$$A_3(\mathbf{k},\beta)=\frac{k_2\sqrt{k_1^2+k_3^2}}{k_1^2}\left(\arctan\frac{\beta k_1-k_2}{\sqrt{k_1^2+k_3^2}}+\arctan\frac{k_2}{\sqrt{k_1^2+k_3^2}}\right)-\frac{k_1^2+k_3^2}{2k_1^2}\ln\left(\frac{k_0^2}{k_0^2-2\beta k_1k_2+\beta^2k_1^2}\right).$$

In order to compute the scalar fluxes and due to the complexity of the above formulas, we present results from numerical integrations of (34) and (35) over all the wave numbers. The evolution of the scalar fluctuation intensities $S^2(\overline{\theta_i^2}-\overline{\theta_i^0\theta_i^0})/G_i^2q_0^2$ is presented in Fig. 9 and that of the normalized scalar fluxes $S\overline{\theta_iu_j}/G_iq_0^2$ in Fig. 10. These figures reveal the following asymptotic behaviors:

$$\frac{S^2}{G_1^2q_0^2}(\overline{\theta_1^2}-\overline{\theta_1^{2}}^0)\sim\beta,\quad\frac{S\overline{\theta_1u_1}}{G_1q_0^2}\to-\ln 2,\quad\frac{S\overline{\theta_1u_2}}{G_1q_0^2}\sim\beta,$$
$$\frac{S^2}{G_2^2q_0^2}(\overline{\theta_2^2}-\overline{\theta_2^{2}}^0)\sim\beta^3,\quad\frac{S\overline{\theta_2u_1}}{G_2q_0^2}\sim\beta,\quad\frac{S\overline{\theta_2u_2}}{G_2q_0^2}\sim-\beta^2.\tag{37}$$

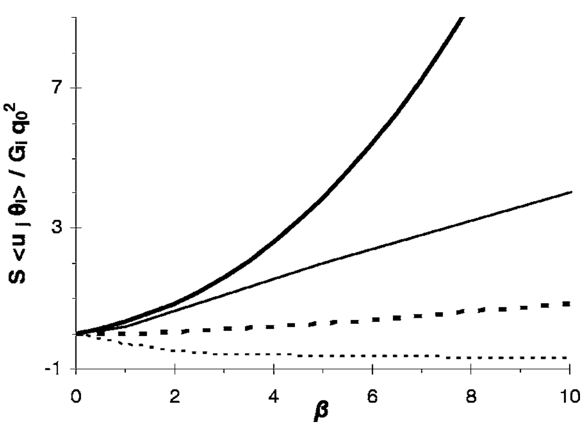

FIG. 10. Time development of the scalar flux components, $S\overline{\theta_1u_1}/G_1q_0^2\to-\ln 2$ (thin dashed line), $S\overline{\theta_1u_2}/G_1q_0^2\sim\beta$ (thin solid line), $S\overline{\theta_2u_1}/G_2q_0^2\sim\beta$ (thick dashed line), $-S\overline{\theta_2u_2}/G_2q_0^2\sim\beta^2$ (thick solid line).

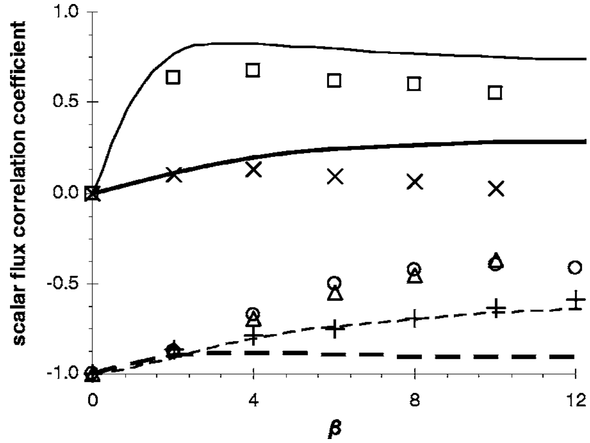

FIG. 11. Time development of the scalar flux correlation coefficients calculated by the inviscid RDT (lines) and the DNS data (symbols) from Brethouwer (Ref. 6) when $\eta=1$ for: $\overline{\theta_1u_2}$ (thin solid line; □), $\overline{\theta_2u_1}$ (thick solid line; ×), $\overline{\theta_1u_1}$ (thin dashed line; △), $\overline{\theta_2u_2}$ (thick dashed line; +). The DNS results for $\overline{\theta_2u_2}$ when $\eta=0$ (○) are also given for comparison.

Recalling that the shear stress component approaches a constant $R_{12}/q_0^2\to-0.25$, the asymptotic limits for the turbulent Prandtl number $\mathrm{Pr}_T=(\overline{u_1u_2}/S)/(\overline{\theta_iu_i}/G_i)$ become $0.25/\ln 2\approx0.36$ for θ_1 and $0.25/\beta^2\to0$ for θ_2. Taking into consideration notation differences, the above asymptotic results (37) take the same form as the ones obtained by Rogers[12] for the case without frame rotation ($\eta=0$). More specifically, it seems that there exists a correspondence between the asymptotic results for the scalar fluxes and variances regarding θ_1 and θ_2 for $\eta=1$ and the ones regarding θ_2 and θ_1 (denoted as θ_2 and θ_4 by Rogers[12]) for $\eta=0$, respectively. For example $S^2(\overline{\theta_2^2}-\overline{\theta_2^{2}}^0)/G_2^2q_0^2(\eta=1,\beta)\sim S^2(\overline{\theta_1^2}-\overline{\theta_1^{2}}^0)/G_1^2q_0^2(\eta=0,\beta)\sim\beta^3$. This asymptotic similarity could be partially expected due to the fact that, the stress components 22 for the case with $\eta=1$ and 11 for the case with $\eta=0$ equal to each other, $R_{11}(\eta=1)=R_{22}(\eta=0)$, for any value of total shear β (as we have already proved). For the components $R_{22}(\eta=1)$ and $R_{11}(\eta=0)$, although there is not such equality, they both tend to evolve linearly with the time. More impressively, the equality between the stress components $R_{11}(\eta=1)=R_{22}(\eta=0)$ can be shown (numerically) to extend to the corresponding scalar flux components, i.e., $S\overline{\theta_1u_1}/G_1q_0^2(\eta=1,\beta)=S\overline{\theta_2u_2}/G_2q_0^2(\eta=0,\beta)$ at any β. This finding is also supported by data from the DNS of Brethouwer.[6] In Fig. 11, the time development of the scalar flux correlation coefficients calculated in this study using the inviscid RDT equations is compared to the DNS data. Despite the contributions from the nonlinear and the viscous terms in the DNS, the similarity of the evolution histories for the correlation coefficients is clear. From the same figure it can be seen that in general the early time response of the scalar fluxes given by the RDT equations is in good agreement with the corresponding DNS results. For values of β larger than 4 though, the correlation coefficients from the RDT analysis tend to constant values that remain somewhat higher than the DNS levels. In the case of $\overline{\theta_1u_2}$ the inviscid RDT predicts a slight decrease but not as rapid as the DNS.

Despite the above mentioned similarities between the development of the scalar field for $\eta=0$ and $\eta=1$, there is one remarkable difference if the ratio of the scalar fluxes is considered, as pointed out by one of the referees. The asymptotic limit for the ratio $\overline{\theta_i u_1}/\overline{\theta_i u_2}\to 0$ when $\eta=1$, and $\overline{\theta_i u_1}/\overline{\theta_i u_2}\to\infty$ when $\eta=0$, implies that the scalar flux vector aligns, in the asymptotic limit, with the x_2 axis in the first case and with the x_1 axis in the second, irrespective of the direction of the mean scalar gradient.

VII. CONCLUSIONS

In this study we investigated the case of nonstratified homogeneous turbulence that is sheared in a frame that counter-rotates with a rate that matches the magnitude of the rotation rate associated with the mean shear ($\eta=1$). This defines the upper unstable limit in terms of the energy growth. Any value of η larger than 1, causes a vanishing turbulence as discussed by Salhi.[5] Through an inviscid RDT analysis, it has been found that in this case $R_{ij}=D_{ij}$ and analytical RDT solutions have been developed for the evolution of both these tensor components. The calculated energy growth proved to tend (quite fast) to a linear form, and it is equally shared between R_{22} and R_{33}. Additionally, we have found that the evolution of the normal stress component $R_{11}(\beta)/q_0^2$ in the counter-rotating case ($\eta=1$) is identical to that of $R_{22}(\beta)/q_0^2$ that can be obtained by integrating the spectral solution reported by Rogers[12] for the case without frame rotation ($\eta=0$). For the remaining stress components, however, no such similarities exist. The analytical solutions of the RDT equations compare very favorably with DNS data for similar conditions. The agreement is especially good in terms of the shear stress. Both the analytical solution and the DNS show a linear growth of the turbulent kinetic energy. A moderate overestimation of the growth rate by the analytical solution as compared to the DNS is attributed almost exclusively to the absence of viscosity. The nonlinearity does not seem to contribute significantly to the difference in growth rate, as it might be expected for these relatively rapid shear rates. In terms of the development of the structure of a passive scalar field with a constant mean gradient, it has been shown that there exist remarkable analogies between this case and the one without any rotation examined by Rogers.[12]

ACKNOWLEDGMENTS

The authors would like to thank Dr. G. Brethouwer for kindly providing the DNS data used for comparisons with the analytical solutions, and the anonymous referees for helpful comments. This work has been performed under the UCY-CompSci project, a Marie Curie Transfer of Knowledge (TOK-DEV) grant (Contract No. MTKD-CT-2004-014199), and under the SBM-EuroFlows project, a Marie Curie IRG grant (Contract No. MIRG-CT-2004-511097) both funded by the CEC under the 6th Framework Program.

APPENDIX: ANALYTICAL INTEGRATIONS OF THE SPECTRAL EXPRESSIONS FOR THE DERIVATION OF THE STRESS COMPONENTS

The integrals (15) in Sec. IV, can be simplified, by excluding the parts of the initial integrands that vanish after the integration over the two angles. We present as an example $R_{12}(\beta)/q_0^2$, which can be written in the form

$$\begin{aligned}\frac{R_{12}(\beta)}{q_0^2}&=\frac{D_{12}(\beta)}{q_0^2}\\&=\int_0^{\pi}\cos\alpha\sin^2\alpha\\&\quad\times\int_0^{2\pi}\frac{-\sin\varphi}{8\pi(A(\alpha,\beta)-B(\alpha,\beta)\sin\varphi)^2}d\varphi d\alpha,\end{aligned}\tag{A1}$$

where $A(\alpha,\beta)=1+\beta^2\cos^2\alpha$ and $B(\alpha,\beta)=\beta\sin 2\alpha$. After the integration of the inner part, $R_{12}(\beta)/q_0^2$ becomes

$$\frac{R_{12}(\beta)}{q_0^2}=\frac{D_{12}(\beta)}{q_0^2}=\int_0^{\pi/2}\frac{B(\alpha,\beta)\cos\alpha\sin^2\alpha}{2(A^2(\alpha,\beta)-B^2(\alpha,\beta))^{3/2}}d\alpha\tag{A2}$$

and by setting $x=\cos\alpha$ the calculation of $R_{12}(\beta)/q_0^2$ reduces to

$$R_{12}(\beta)/q_0^2=\beta\int_0^1\frac{x^4-x^2}{(C(\beta)x^4-D(\beta)x^2+1)^{3/2}}dx,\tag{A3}$$

where $C(\beta)=\beta^4+4\beta^2$, $D(\beta)=2\beta^2$. The solution of the above integral yields

$$\begin{aligned}\frac{R_{12}(\beta)}{q_0^2}&=\frac{D_{12}(\beta)}{q_0^2}\\&=\frac{-(\beta^2+1)}{8\beta}+\frac{i\beta(3+\beta^2)E_1(\beta)}{8\beta(\beta-2i)\sqrt{-\beta(\beta+2i)}}\\&\quad+\frac{2(\beta-i)^2E_2(\beta)}{8\beta(\beta-2i)\sqrt{-\beta(\beta+2i)}}.\end{aligned}\tag{A4}$$

In the above, the expressions $E_1(\beta)$ and $E_2(\beta)$ are functions of elliptic integrals according to $E_1(\beta)=E[m(\beta),\varphi(\beta)]$, $E_2(\beta)=F[m(\beta),\varphi(\beta)]$, where F, E are elliptic integrals of the first and the second kind, respectively, with the arguments $\varphi=\arcsin\sqrt{\beta(\beta+2i)}$ and $m=(\beta-2i)/(\beta+2i)$. For values of the total shear larger than 1.55, we must take care to continue by choosing the appropriate branches of the elliptic integrals.

Following a similar procedure, $R_{11}(\beta)/q_0^2$ becomes

$$\frac{R_{11}(\beta)}{q_0^2} = \frac{D_{11}(\beta)}{q_0^2} = \beta\frac{R_{12}(\beta)}{q_0^2} + \frac{1}{8\pi}\int_0^{\pi}\int_0^{2\pi}\frac{\sin^3\alpha}{(1-2\beta\cos\alpha\sin\alpha\sin\varphi+\beta^2\cos^2\alpha)^2}d\varphi d\alpha. \tag{A5}$$

After integrating the inner part and applying appropriate transformations $R_{11}(\beta)/q_0^2$ is calculated through

$$\frac{R_{11}(\beta)}{q_0^2} = \frac{D_{11}(\beta)}{q_0^2} = \frac{1}{2}\int_0^1\frac{1-x^2-\beta^2x^2+\beta^2x^4}{(C(\beta)x^4-D(\beta)x^2+1)^{3/2}}dx, \tag{A6}$$

which results in the final expression

$$\frac{R_{11}(\beta)}{q_0^2} = \frac{D_{11}(\beta)}{q_0^2} = \frac{-E_1(\beta)+(\beta^2+1-2i\beta)E_2(\beta)}{4\beta(\beta-2i)\sqrt{\beta(\beta+2i)}}. \tag{A7}$$

For $R_{22}(\beta)/q_0^2$ it can be shown (however this demands some effort) that

$$\frac{R_{22}(\beta)}{q_0^2} = \frac{D_{22}(\beta)}{q_0^2} = \frac{1}{8\pi}\int_0^{\pi}\int_0^{2\pi}\frac{\sin^3\alpha}{(1-2\beta\cos\alpha\sin\alpha\sin\varphi+\beta^2\cos^2\alpha)^2}d\varphi d\alpha, \tag{A8}$$

which via (A5) gives

$$\frac{R_{22}(\beta)}{q_0^2} = \frac{D_{22}(\beta)}{q_0^2} = \frac{R_{11}(\beta)}{q_0^2} - \beta\frac{R_{12}(\beta)}{q_0^2} = \frac{D_{11}(\beta)}{q_0^2} - \beta\frac{D_{12}(\beta)}{q_0^2} \tag{A9}$$

and thus, $R_{22}(\beta)/q_0^2$ is calculated through the combination of (A7) and (A4). Finally, $R_{33}(\beta)/q_0^2$ can be written as

$$\frac{R_{33}(\beta)}{q_0^2} = \frac{D_{33}(\beta)}{q_0^2} = \frac{1}{8\pi}\int_0^{\pi}\int_0^{2\pi}\frac{\sin a(1-\sin^2\alpha\cos^2\varphi)}{(1-2\beta\cos\alpha\sin\alpha\sin\varphi+\beta^2\cos^2\alpha)^2}d\varphi d\alpha, \tag{A10}$$

which results in

$$R_{33}(\beta)/q_0^2 = \frac{1}{4} + \frac{\beta^2+1}{8} + \frac{(\beta^2+1)(2-i\beta)E_1(\beta)-2(\beta^2+1)E_2(\beta)}{8\beta\sqrt{-\beta(\beta+2i)}}. \tag{A11}$$

[1] M. M. Rogers and P. Moin, "The structure of the vorticity field in homogeneous turbulent flows," J. Fluid Mech. **176**, 33 (1987).
[2] J. M. Lee, J. Kim, and P. Moin, "Structure of turbulence at high shear rate," J. Fluid Mech. **216**, 561 (1990).
[3] J. Bardina, J. H. Ferziger, and W. C. Reynolds, "Improved turbulence models based on large-eddy simulation of homogeneous incompressible turbulent flows," Technical Report No. TF-19, Department of Mechanical Engineering, Stanford University, Stanford, CA (1983).
[4] A. Salhi and C. Cambon, "An analysis of rotating shear flow using linear theory and DNS and LES results," J. Fluid Mech. **347**, 171 (1997).
[5] A. Salhi, "Similarities between rotation and stratification effects on homogeneous shear flow," Theor. Comput. Fluid Dyn. **15**, 339 (2002).
[6] G. Brethouwer, "The effect of rotation on rapidly sheared homogeneous turbulence and passive scalar transport. Linear theory and direct numerical simulation," J. Fluid Mech. **542**, 305 (2005).
[7] A. A. Townsend, *The Structure of Turbulent Shear Flow*, 2nd ed. (Cambridge University Press, Cambridge, 1976).
[8] J. C. R. Hunt, "A review of the theory of rapidly distorted turbulent flow and its applications," Fluid Dyn. Res. **9**, 121 (1978).
[9] A. M. Savill, "Recent developments in rapid distortion theory," Annu. Rev. Fluid Mech. **19**, 531 (1987).
[10] J. C. R. Hunt and D. J. Carruthers, "Rapid distortion theory and the 'problems' of turbulence," J. Fluid Mech. **212**, 497 (1990).
[11] C. Cambon and J. F. Scott, "Linear and nonlinear models of anisotropic turbulence," Annu. Rev. Fluid Mech. **31**, 1 (1999).
[12] M. M. Rogers, "The structure of a passive scalar field with a uniform mean gradient in rapidly sheared homogeneous turbulent flow," Phys. Fluids A **3**, 144 (1991).
[13] O. Metais, C. Flores, S. Yanase, J. J. Riley, and M. Lesieur, "Rotating free-shear flows. Part 2. Numerical simulations," J. Fluid Mech. **293**, 47 (1995).
[14] S. C. Kassinos and W. C. Reynolds, "A structure based model for the rapid distortion of homogeneous turbulence," Technical Report No. TF-61, Department of Mechanical Engineering, Stanford University, Stanford, CA (1994).
[15] S. C. Kassinos and W. C. Reynolds, "A particle representation model for the deformation of homogeneous turbulence," in *Annual Research Briefs 1996* (Stanford University and NASA Ames Research Center, Center for Turbulence Research, Stanford, 1996), pp. 31–50.
[16] S. C. Kassinos and W. C. Reynolds, "Structure-based modeling for homogeneous MHD turbulence," in *Annual Research Briefs 1999* (Stanford University and NASA Ames Research Center, Center for Turbulence Research, Stanford, 1999), pp. 301–315.
[17] R. S. Rogallo, "Numerical experiments in homogeneous turbulence," NASA Tech. Memo. 81315 (1981).
[18] P. Bradshaw, "The analogy between the streamline curvature and buoyancy in turbulent shear flow," J. Fluid Mech. **36**, 177 (1969).
[19] S. C. Kassinos, W. C. Reynolds, and M. M. Rogers, "One-point turbulence structure tensors," J. Fluid Mech. **428**, 213 (2001).